Article

An Analytical Study of the Effects of Kinematic Parameters on the Motion Stability of a 3-RPR Parallel Manipulator in Singular Configurations

Yu-Tong Li and Yu-Xin Wang *

China University of Petroleum (East China), Qingdao 266580, China; lytong_b@163.com
* Correspondence: strath_tj@hotmail.com

Abstract: Due to the Jacobian matrix rank reduction near singularities, applying numerical methods to study PMs' motion stability at singularities is quite difficult. As a result, there is a scarcity of literature on the investigation of PMs' dynamic behaviors near singularities and the influence of kinematic parameters on the motion stability of PMs. To address the research gap related to the above issues, based on the Gerschgorin perturbation method, Hurwitz exact approach, and the Lyapunov dynamic stability theory, the influence of kinematic parameters and external loads on a PM's motion stability at singularities is studied for the first time. The theoretical analysis results reported in this paper reveal many previously undiscovered features beyond those derived from previous numerical methods, and indicate the limitations of some widely accepted statements. For example, increasing the angular speed of the movable platform can expand the range of the external loads that meet the motion stability at singular configurations. The prevailing notion in prior research that PMs are unable to support external loads in the direction of the gained DoF at singular configurations is only partially accurate. This pioneering research establishes a theoretical foundation for exploring a new real-time approach to avoid dynamic singularities by fully exploiting the influence mechanisms of kinematic parameters on PMs' dynamic stability at singularities.

Keywords: dynamical motion stability; kinematic singularities; kinematic parameters; nonlinear stability theory; parallel manipulator (PM)

MSC: 37G10; 37N30; 70E50; 65P40

1. Introduction

Parallel manipulators (PMs) offer a multitude of benefits over serial manipulators, such as an exceptional load-carrying capacity, precision, and rigidity. Nevertheless, PMs present a significant obstacle due to singularities within their workspace [1,2]. Singular configurations can result in PMs instantaneously gaining or losing a degree of freedom (DoF), restricting their ability to withstand external forces or torque in specific directions. Because singularities can adversely impact PMs' static properties and motion control, avoiding singularities in their workspace is of primary importance [3–5].

The singularity-free design approaches [6–8] attempt to eliminate singularities by selecting a workspace region during the design stage. Another approach involves identifying the singularity-free region [9–12], which helps determine the subsets of the workspace where the robot can move freely without encountering singularities. While PM works inside the singularity-free region, it can move freely without encountering singularities. Because the singular loci [13] are closely related to the amplitude of the end-effector orientation parameters, the singularity-free workspace will be significantly reduced if the orientation parameters change over a relatively large scope. Singularity-free path planning [14–16] is a commonly used method to avoid singularities when performing a specific task within a given workspace. The trajectory planning algorithms aim to create a path that connects the

initial configuration to the final configuration without encountering a singularity. However, in cases where the initial and final configurations are located in different regions separated by singularity distribution hypersurfaces [13], determining a singularity-free path is sometimes impossible. This challenge is further complicated because the singularity-free regions are not continuous.

Introducing redundancies in a PM can help avoid singularities by adding an actuator to one of the passive joints or introducing additional legs into the manipulator [17]. The PM's kinematic properties at singular configurations can then be modified and improved. This approach has been studied in various studies [18–20], including reconfigurable PMs [3,21]. Gosselin et al. [22] found that incorporating active masses to select links can alter the center locations of masses and other dynamic properties of PMs. Building on this concept, Parsa et al. [23] implemented it to enhance the dynamic properties of the planar 3-RRR PM during tasks involving sharp turns. In another study [24], the authors investigated the feasibility of implementing a desired trajectory containing direct kinematic singularities for a planar 2-RPR PM. They applied reconfigurable active masses to help the PM cross these kinematic singular configurations. The theoretical investigation demonstrated that by applying reconfigurable mass parameters, the PM could cross kinematic singular configurations. Agarwal et al. [25] developed a strategy to prevent dynamic singularities in PMs. They used an artificial potential function that changes a PM's behavior when it approaches singularities. This control scheme enables the PM to avoid singularities without deviating off the path, which makes it suitable for dynamic singularity avoidance within workspaces. However, the proposed scheme has one drawback: it sacrifices one DoF to avoid the singularities in the low-dimensional task space. However, introducing redundancy [17–21] or active mass [22–25] will increase the complexity of the online control of PMs and the system's cost. In aerospace applications, the addition of redundancy or active mass is restricted due to the increased weight and complexity of the control system they cause.

Measuring the closeness to singularities based on the characteristics of PMs at near-singular configurations, such as Jacobian-based indices [26] and the transmission index [27], is a way to prevent a manipulator from falling into static singularities. Saafi et al. [28] used force sensors to prevent PMs from falling into a single configuration, considering that a small force or torque applied in a particular direction related to the obtained degrees of freedom will produce a massive force in a linkage of a singular configuration. However, it is difficult for motion/force or Jacobian matrix-based indicators to accurately capture all singularities in the vicinity of PM's singular configurations due to their sudden changes in values [29]. Hu et al. [30] proposed an offline strategy to measure the closeness to singularity and avoid singularity for a planar robot with kinematic redundancy based on the performance of the kinematics and dynamics. Meanwhile, Yao et al. [31] introduced a geometric algebra index for measuring the proximity to a PM's singularities by determining the ratio of the non-singularity workspace volume, which has a precise geometrical and physical interpretation. Lastly, Kapilavai and Nawratil [32] proposed extrinsic metrics that can identify the configurations closest to singularities, utilizing algorithms from numerical algebraic geometry implemented in Bertini's software package (Bertini 1.6v) [33]. The singularity-free methods mentioned in [3,4,29–32] require offline computations before execution whenever the path, workspace, or end-effector orientation parameters change. However, the recalculation process will reduce the method's flexibility and lead to a loss of optimal adjustment time, which can be crucial in aerospace applications and could result in severe disasters. In such a scenario, while a robotic system deviates from its pre-programmed path and encounters a singularity, it may be unable to reposition itself to avoid upcoming singularities along its trajectory.

It is often challenging to identify all singularities in the whole workspace analytically. Thus, singularity-free operations should be performed dynamically without prior knowledge of the locations of the gain-type singularities inside the workspace. Moreover, in aviation and space explorations, adaptive real-time singularity avoidance is essential for equipment safety with driving PMs [34]. In view of the adverse effects of introducing

redundancy and mass on the system weight and complexity and offline recalculation reducing control flexibility and robustness, the proposal of a real-time control method that can realize PMs' adaptive singularity avoidance without offline calculation and the introduction of redundancy and mass is required.

In most cases, PMs pass by their singular configurations dynamically rather than staying at the singular configurations. In such situations, kinematic parameters can affect the dynamic stability, particularly in singular configurations such as a parallelogram mechanism. At a certain velocity, it can pass through the singular configuration, where the crank coincides with the ground, with predetermined motion and load capacity. Inspired by this case, the motion stability of a planar 3-RPR PM dynamics system at singular configurations corresponding to the kinematic parameters was investigated [35] by a numerical analysis of the eigenvalues of the linear approximation dynamical system at the singularities based on Lyapunov's stability theorem [36].

This paper builds upon the prior research by using an analytical approach to investigate the relationship between kinematic parameters and a PM's dynamic stability at singular configurations. The main goal is to comprehensively understand how each kinematic parameter affects motion stability at singularities. This study aims to develop a more efficient and user-friendly method suitable for aerospace applications that can dynamically and adaptively avoid singularities in real time based on sensing input parameters without offline calculations. To the best of the author's knowledge, no existing literature has considered the system's dynamic characteristics when constructing singularity-free approaches and studying PMs' motion stability at singularities.

2. Materials and Methods

2.1. Linear Approximation Dynamics System of the 3-RPR PM

To analyze the motion stability of the 3-RPR PM dynamics system at the singular configuration related to the system's kinematic parameters, the 3-RPR PM should be dispersed into a system of particles, as shown in Figure 1 in Ref. [35]. The continuous mass of the movable platform is dispersed into three concentrated masses, m_1, m_2, and m_3, which are located at three respective revolute (R) joints B_i on the movable platform. The distances between the two revolute joints on the movable platform are b_1, b_2, b_3, respectively. The prismatic pair (P), such as the prismatic pair related to the input parameter l_1, is dispersed into two concentrated masses, m_4 and m_7, at point D_1 and point C_1, respectively. The distance from D_1 to the fixed joint A_1 is represented by d_1; the distance from C_1 to the revolute joint B_1 is represented by c_1. The symbols representing the other two branches, l_2 and l_3, have the same meaning. The external forces $\overrightarrow{F}_i$, $(i = 1, 2, 3)$ act on the movable platform via the revolute joints, B_i, $(i = 1, 2, 3)$, respectively. Using the first-class Lagrange approach, the dynamics equation of this discrete system of particles is modeled.

Select the center coordinates x_c, y_c of the moveable platform and the rotation angle θ as the generalized coordinates $q = \{q_1, q_2, q_3\}^T = \{x_c, y_c, \theta\}^T$. All coordinates of discrete concentrated masses of the system can be represented by this set of generalized coordinates. The geometric constraint equations for the 3-RPR PM are:

$$\begin{cases} f_{4i-3} = (\boldsymbol{B}_{i+1} - \boldsymbol{B}_i)^T (\boldsymbol{B}_{i+1} \big|_{if\ i+1>3, i+1=i-2} - \boldsymbol{B}_i) - b_i^2 = 0 \\ f_{4i-2} = (\boldsymbol{D}_i - \boldsymbol{A}_i)^T (\boldsymbol{D}_i - \boldsymbol{A}_i) - d_i^2 = 0 \\ f_{4i-1} = (\boldsymbol{B}_i - \boldsymbol{C}_i)^T (\boldsymbol{B}_i - \boldsymbol{C}_i) - c_i^2 = 0 \qquad i = 1, 2, 3 \\ f_{4i} = \boldsymbol{B}_i \boldsymbol{C}_i / / \boldsymbol{D}_i \boldsymbol{A}_i \end{cases} \quad (1)$$

The constraint forces caused by the above geometric constraints acting on each set of generalized coordinates are (A_{rs} see Appendix A)

$$
\begin{cases}
B_{ri}(q_1, q_2, q_3, t) = \sum\limits_{s=1}^{9\times 2} A_{rs} \dfrac{\partial u_s}{\partial q_i}, & r = 1, \dots, 12 \\
\sum\limits_{s=1}^{9\times 2} \dfrac{\partial f_r}{\partial u_s} du_s = \sum\limits_{s=1}^{9\times 2} A_{rs} du_s = 0, & u_s \in \{x_i, y_i\}_{i=1,2,\dots,9}
\end{cases}
\tag{2}
$$

Considering that the external forces $\vec{F}_1$, $\vec{F}_2$, $\vec{F}_3$ and the gravities act on the three concentrated particles m_1, m_2, m_3, respectively, the second Lagrange dynamics equation for the 3-RPR PM is

$$
\begin{cases}
\dfrac{d}{dt}\left(\dfrac{\partial T}{\partial \dot{q}_i}\right) - \dfrac{\partial T}{\partial q_i} = Q_i + \sum\limits_{r=1}^{12} \lambda_r B_{ri} & (i = 1, 2, 3) \\
\sum\limits_{i=1}^{3} B_{ri} \dot{q}_i + B_r = 0 (r = 1, \dots, 12)
\end{cases}
\tag{3}
$$

Eliminate all of the Lagrange multipliers in Equation (3), and let the non degenerate matrix be $D = \{d_{ij}\}_{3\times 3}$ and let the integrated expression of Equation (3) be $Dq = B(q, \dot{q}, t)$. Let $\tau^T D \tau q = \tau^T B(q, \dot{q}, t)\tau$, then the second order of uncoupled expression for Equation (3) is

$$
\begin{cases}
\ddot{q}_1 = \phi_1(\dot{q}^2, q, q^2, \dots, q^{12}, \alpha_1, \alpha_2, \alpha_3, F_1, F_2, F_3) \\
\ddot{q}_2 = \phi_2(\dot{q}^2, q, q^2, \dots, q^{12}, \alpha_1, \alpha_2, \alpha_3, F_1, F_2, F_3) \\
\ddot{q}_3 = \phi_3(\dot{q}^2, q, q^2, \dots, q^{12}, \alpha_1, \alpha_2, \alpha_3, F_1, F_2, F_3)
\end{cases}
\tag{4}
$$

Substitute the generalized coordinates $q_0 = \{x_{c0},\ y_{co},\ \theta_{c0}\}^T$ at the singular configuration into the above equation, and give up higher 7-order terms; the dynamics equation at the singular configuration related to the generalized coordinates q is

$$
\begin{cases}
\ddot{q}_1 = \varphi_1(\dot{q}^2, q, q^2, \dots, q^6, \alpha_1, \alpha_2, \alpha_3, F_1, F_2, F_3) \\
\ddot{q}_2 = \varphi_2(\dot{q}^2, q, q^2, \dots, q^6, \alpha_1, \alpha_2, \alpha_3, F_1, F_2, F_3) \\
\ddot{q}_3 = \varphi_3(\dot{q}^2, q, q^2, \dots, q^6, \alpha_1, \alpha_2, \alpha_3, F_1, F_2, F_3)
\end{cases}
\tag{5}
$$

The dynamic stability of differential dynamics systems mainly depends on its lower-order dynamic terms [36]. Here, using the Taylor series method to obtain the lower-order terms, the linear approximation dynamics system of the 3-RPR PM represented by Equation (5) in the vicinity of the singular configuration is

$$
\dot{x} = Ax + G(x, t) + O(\|x\|^3)
\tag{6}
$$

Here, $A = \begin{pmatrix} 0 & I \\ A_1 & C \end{pmatrix}$, $A_1 = \{a_{ij}\}_{3\times 3}$, $C = (c_{ij})_{3\times 3}$, $\Psi \in R^{6\times 6}$, and $G(x, t) = x^T \Psi x$ is the secondary homogeneous polynomial related to $x = \{q_1, q_2, q_3, \dot{q}_1, \dot{q}_2, \dot{q}_3\}^T$.

2.2. Analytical Methods

This study aims to develop a new approach for a PM to operate robustly and adaptively in online control mode throughout its entire workspace by sensing and adjusting the primary kinematic parameters without encountering the singularity problem. The PM should be discretized into a system of discrete particles. Then, its detailed analytical uncoupled quadratic dynamical model should be constructed using the first-class Lagrange method or alternative analytical approaches. Next, the PM's analytical dynamic model should be reduced into a linear approximation dynamic system with the lower-order terms based on the Taylor series method. This is because the motion stability of differential dynamic systems primarily depends on their lower-order dynamic terms. However, using

analytical techniques to model the dynamics of PMs with multiple degrees of freedom is complicated. Usually, numerical methods, such as the universal unfolding method [37], are required to simplify this by treating the model as a linear polynomial in the germ space of the singular point so that follow-up analytical procedures can be applied. Finally, the motion stability of PMs at singular configurations corresponding to joint kinematic parameters should be investigated analytically based on the eigenvalue equations determined by the linear approximation dynamic system. Three analytical approaches were adopted here: direct analysis, the Gerschgorin circle-based approximate analysis, and the Hurwitz criterion-based exact analysis.

The analytical process shown in Figure 1 encounters two main challenges. The first is eliminating all acceleration terms and multipliers in the first-class Lagrange equation. The second challenge is to obtain an explicit analytical expression of the eigenvalue equation, which governs the motion stability of a PM dynamic system at singular configurations corresponding to the joint kinematic parameters. The former is quite technical, while the latter is more complicated for complex PMs, such as a 6-SPS PM. Different from the singular configuration determined by the pose parameters of the movable platform, the singular configuration in this paper is closely related to the joint parameters, such as the input parameters [38], treated as the bifurcation parameters. Thus, the method to avoid singularity can be constructed by detecting the input parameters. However, the singular configuration determined by pose parameters cannot be used to construct this type of singularity-free approach.
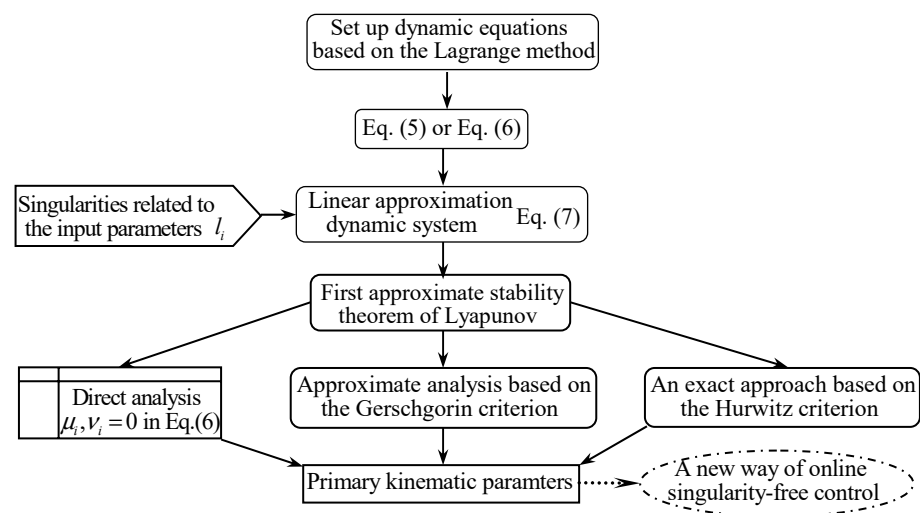

Figure 1. Analytical approaches to determine primary kinematic parameters for constructing new singularity-free approach for aerospace applications.

3. Results

3.1. Unstable Motion Related to $q_{bi} = m_i(\mu_i - v_i) = 0$

According to the first approximate stability theorem of Lyapunov [36], if each of the eigenvalues of the linear approximation for the 3-RPR PM dynamics system has a negative real part at a singular configuration, then the motion of the dynamics system at a singular configuration is stable. Thus, the problem of evaluating whether the PM can pass by the singular configuration dynamically with a definite anti-disturbance capability is transformed to estimating whether each of the eigenvalues of the linear approximation dynamics system has a negative real part. If all the eigenvalues have negative real parts, the system's motion at the singular configuration is stable; consequently, the manipulator can pass by the singular configuration with the desired motion and anti-disturbance capability.

When the coordinates of three revolute joints $B_i = \{x_i(t), y_i(t)\}_{i=1,2,3}^T$ on the movable platform are taken as the generalized coordinates, the dynamic model of the 3-RPR PM can be built similarly, as follows:

$$M\ddot{u} = F_G + Pq_b + Qq_d \tag{7}$$

where $M = diag\{m_1, m_1, m_2, m_2, m_3, m_3\}$, $\ddot{u} = \{\ddot{x}_1, \ddot{y}_1, \ddot{x}_2, \ddot{y}_2, \ddot{x}_3, \ddot{y}_3\}^T$, $P = \{p_{ij}\}_{6\times3}$, $Q = \{q_{ij}\}_{6\times3}$.

$$q_b = \left\{ \begin{array}{c} q_{b1} \\ q_{b2} \\ q_{b3} \end{array} \right\} = \left\{ \begin{array}{c} m_1(\dot{l}_1{}^2 - \dot{x}_1{}^2 - \dot{y}_1{}^2 + l_1\ddot{l}_1) \\ m_2(\dot{l}_2{}^2 - \dot{x}_2{}^2 - \dot{y}_2{}^2 + l_2\ddot{l}_2) \\ m_3(\dot{l}_3{}^2 - \dot{x}_3{}^2 - \dot{y}_3{}^2 + l_3\ddot{l}_3) \end{array} \right\}$$

$$q_d = \left\{ \begin{array}{c} q_{d1} \\ q_{d2} \\ q_{d3} \end{array} \right\} = \left\{ \begin{array}{c} F_1(\cos\alpha_1 x_1 + \sin\alpha_1 y_1) - m_1 g y_1 \\ -a_0 F_2 \cos\alpha_2 + b_0(m_2 g - F_2\sin\alpha_2) + \cos\alpha_2 F_2 x_2 + \sin\alpha_2 F_2 y_2) - m_2 g y_2 \\ F_3(\cos\alpha_3 x_3 + \sin\alpha_3 y_3 - a\cos\alpha_3) - m_3 g y_3 \end{array} \right\}$$

$$F_G = \{\cos\alpha_1 F_1, \sin\alpha_1 F_1 - m_1 g, \cos\alpha_2 F_2, \sin\alpha_2 F_2 - m_2 g, \cos\alpha_3 F_3, \sin\alpha_3 F_3 - m_3 g\}^T$$

p_{ij}, q_{ij} are parameters related to $x_i(t)$, $y_i(t)$ and the dimensions of the 3-RPR PM. $\mu_i = \dot{l}_i{}^2 + l_i\ddot{l}_i$ in q_{bi} are known as the input kinematic parameters, and $v_i = \dot{x}_i{}^2 + \dot{y}_i{}^2$ are the kinematic parameters of the joint velocities; thus, $q_{bi} = m_i(\mu_i - v_i)$.

Equation (7) provides a comprehensive understanding of how input kinematic parameters, joint velocities, external loads, and gravities interact to influence the PM's dynamic properties. The uncoupled quadratic equation, without multipliers, offers a clear insight into the impact of these variables on the PM's dynamic properties throughout its workspace, especially near singular configurations. This analytical expression provides a necessary means or bridge to investigate the motion stability of the 3-RPR PM at singular configurations corresponding to the system's input kinematic parameters and joint velocities.

By employing the Taylor series method, a similar linear approximation dynamics system equivalent to Equation (6) can be obtained in the vicinity of the singular configuration with respect to Equation (7). In Equation (7), both μ_i and v_i have impacts on the eigenvalues of matrix A. If $q_{bi} = m_i(\mu_i - v_i)$ causes at least one of the eigenvalues to have a nonzero positive real part, the dynamic response or motion of the 3-RPR PM at its singular configurations will become unstable. On the other hand, if μ_i and v_i satisfy the condition $q_{bi} = 0$, all the elements in the sub-matrix of A_1 of the linear approximate system matrix A related to Equation (6) will be zero. Consequently, all the eigenvalues of matrix A will also be zero. Based on the theorem of Lyapunov, the motion of the 3-RPR PM at its singular configuration becomes unstable. There are three types of cases related to this situation.

i. $v_i = 0$ and $\dot{l}_i = \ddot{l}_i = 0$.

In this case, the position of the PM's movable platform is fixed (the manipulator remains stationary). According to the stability theorem, the motion of the dynamic system at the singular configuration related to the static state is unstable. When the lengths of all the input legs (or parameters) are locked, the movable platform will gain a single DoF around the center mid-perpendicular of the movable platform when subjected to disturbances, and the movable platform will lose control. This type of static singularity is categorized as a type II singularity and has been extensively studied by researchers. The literature on singularity-free strategies for PMs has primarily focused on addressing this type of singularity.

ii. $v_i = 0$, $\mu_i = \dot{l}_i{}^2 + l_i\ddot{l}_i = 0$, and $\dot{l}_i \neq 0$, $\ddot{l}_i \neq 0$.

When the input kinematic parameters of the 3-RPR PM dynamics system satisfy $\mu_i = \dot{l}_i{}^2 + l_i\ddot{l}_i = 0$, and the movable platform is at its instantaneous static stage, $v_i = 0$, the system's motion at its singular configurations becomes unstable. This stresses that the trajectory of the joints will be involved in the motion stability of the dynamics system at the singular configurations. However, there is currently no literature in the field of PMs

that discusses the trajectory of the joints in relation to PMs' motion stability at singular configurations, or the exclusion of singularities by adjusting the kinematic parameters of the inputs and/or the joint velocities.

iii. $\mu_i = v_i$, and $\mu_i \neq 0$, $v_i \neq 0$, then $q_{bi} = m_i(\mu_i - v_i) = 0$.

This case corresponds to the correlation between the input kinematic parameters and the joint velocities. In this situation, the movable platform will lose control in singular configurations under external disturbances. To improve the performance of the PM at singular configurations, for example, the motion stability, including anti-disturbances and/or the load capability, preventing the above correlation from emerging while controlling a PM to pass by a singular point in the workspace is desirable. None of the literature in the relevant field mentions or addresses this type of singularity.

3.2. Stable Motion Related to $q_{bi} = m_i(\mu_i - v_i) \neq 0$

The direct analysis in Section 3.1 confirms that the input kinematic parameters and the joint velocities impact the dynamic system's motion stability at singular points. By applying Lyapunov's stability theorem, the motion stability of the PM at singular configurations was studied [35] by analyzing the eigenvalues of the linear approximation of the dynamical system related to Equation (6) at the singularities. It was demonstrated that the motion stability of the PM dynamical system at the singularity can be effectively improved by separately or jointly adjusting the input kinematic parameters and the joint velocities. In particular, increasing the angular speed of the movable platform in the appropriate rotation direction and adjusting the joint velocities to move the absolute velocity center of the movable platform away from the intersecting point of the three driving legs by a certain distance can improve the motion stability of the dynamic system at the singular configuration.

3.2.1. Movable Platform's Instantaneous Center

To study the motion stability relative to the position of the instantaneous center of absolute velocity of the movable platform, let x_0, y_0 represent the instantaneous center of absolute velocity of the movable platform, and let ω represent the angular speed of the movable platform around the center; thus, the velocities of the joints are $\dot{x}_{i0} = -\omega(y_i - y_0)$ and $\dot{y}_{i0} = \omega(x_i - x_0)$. Without the loss of generality, let $\mu_i = \dot{l}_i^2 + l_i \ddot{l}_i$ in $q_{bi} = m_i(\mu_i - v_i)$ be constant. The polynomial of the eigenvalues determined by the linear approximation of the 3-RPR PM dynamics system of Equation (6) with respect to the instantaneous center of absolute velocity x_0, y_0 and the angular speed ω can be obtained. The distributions of the real parts of eigenvalues corresponding to the coordinates of the instantaneous center of absolute velocity x_0, y_0 are shown in Figure 2a.

In this figure, the angular speed of the movable platform is constant, $\omega = \omega_0 \neq 0$, and S is the instantaneous rotation center of the gained DoF of the movable platform at the singular configuration in which the three driving legs of the 3-RPR PM intersect at this point. At this singular configuration, by fixing the lengths of legs l_1, l_2 and releasing leg l_3, the free-moving trace of joint B_3 on the movable platform osculates with the arc centered at A_3 with radius l_3. While fixing the lengths of all three input legs, the movable platform can still rotate around point S. This rotation is a gained DoF. Correspondingly, the absolute value of the negative real part of eigenvalue λ_1 is close to its minimum value near the point S (singular point), and its absolute value along line SA_2 is even smaller than in other regions. Therefore, the motion stability of the 3-RPR PM at the singular configuration is worse if the movable platform's instantaneous center of absolute velocity is located near line SA_2, especially near the intersecting point S.
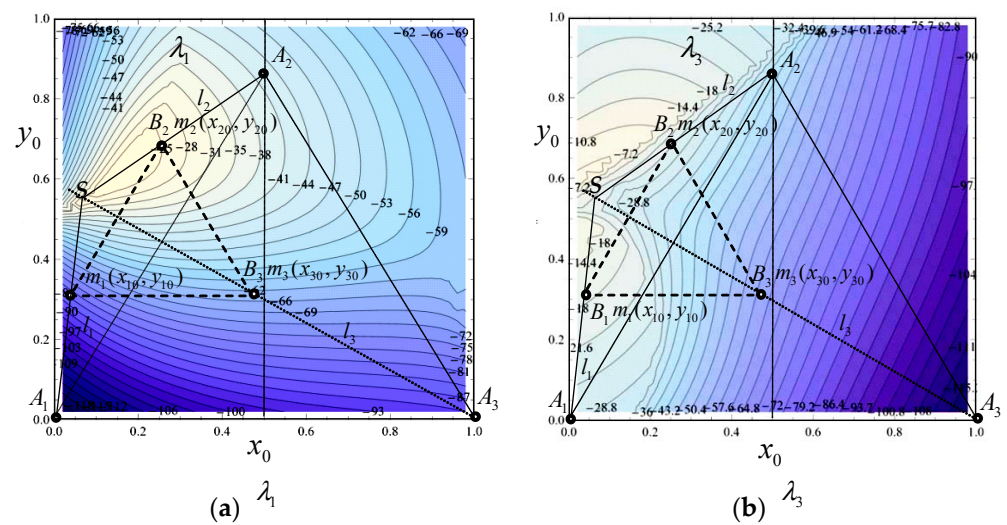
Figure 2. Motion stability related to the instantaneous center of absolute velocity of the movable platform.

The real part distributions of other eigenvalues have the same features as eigenvalue λ_1, such as the distribution of eigenvalue λ_3, as shown in Figure 2b. Along line SA_2 and line SA_1, the absolute value of the negative real part of the eigenvalue λ_3 is smaller than in other areas. In particular, in the vicinity of the singular configuration corresponding to the intersecting point S, the absolute value of the negative real part is close to its minimum. However, when the instantaneous center of the absolute velocity of the movable platform moves away from the intersecting point S and toward the fixed joint A_3, which is the farthest joint from the intersecting point S of the three driving legs, the absolute value of the negative real part of eigenvalue λ_3 increases; correspondingly, the motion stability of the system at the singular configuration is enhanced. In addition, the closer the PM is to the singular position, the smaller the value of the negative real part of the eigenvalues becomes, and the dynamic stability of the 3-RPR PM worsens. However, when the absolute instantaneous velocity center of the movable platform is far away from point S along with line SA_3, the dynamic stability of the system will be enhanced. From Figure 2, it can be deduced that for 3-RPR PM, if the movable platform's absolute velocity instantaneous center is close to the line from the intersecting point S of the three driving legs to the nearest joint on the platform, the dynamic system's motion stability at the singular configuration will be at its worst. Conversely, if the absolute velocity center is farther from point S to the farthest fixed joint, the motion stability at the singular configuration will improve. Therefore, it is desirable to allow the instantaneous center of the absolute velocity of the movable platform to be far away from the instantaneous rotation center of the gained degree of freedom of the movable platform at the singular configuration while planning the joint trajectory or the actual control of the PM.

3.2.2. Velocity of the Mass Center $(\dot{x}_c, \dot{y}_c)$

Using the first approximate stability Lyapunov criterion to analyze the motion stability of the PM at singular configurations, corresponding to velocities and external forces directly, for example, through constructing the Lyapunov potential function, is quite complex and impractical. In this case, the perturbation analysis method based on the Gerschgorin circle theorem is employed to examine the motion stability of the PM at singular configurations $(x_{c0},\ y_{c0},\ \theta_{c0}) = (0.2516,\ 0.4372,\ 0)$ [38] related to the velocities and external forces by investigating the approximate distribution of the eigenvalues.

$$\lambda^3 + C_2(F,\ \alpha,\ \dot{q}_c^2,\ \dot{q}_c)\lambda^2 + C_1(F^2,\ F,\ \alpha,\ \dot{q}_c^4,\ \dot{q}_c^2,\ \dot{q}_c)\lambda + C_0(F^4,\ F^3,\ F^2,\ F,\ \alpha,\ \dot{q}_c^4,\ \dot{q}_c^3,\ \dot{q}_c^2,\ \dot{q}_c) = 0 \quad (8)$$

Here, $\{\dot{x}_c, \dot{y}_c\}^T$ represents the initial velocities of the mass center of the movable platform, $\alpha = \{\alpha_1, \alpha_2, \alpha_3\}^T$, $q_c^m = \left\{ \left. \dot{x}_c^i \, \dot{y}_c^j \, \dot{\theta}_c^{m-i-j} \right|_{i=1\sim m, \, j=1\sim m-i} \right\}^T$, and $F^m = \left\{ \left. F_1^i \, F_2^j \, F_3^{m-i-j} \right|_{i=1\sim m, \, j=1\sim m-i} \right\}^T$.

Suppose that $\boldsymbol{B} = (b_{ij})$ is a plural matrix in the n-order plural plane; the n Gerschgorin circles in the complex plane are

$$G_i(\boldsymbol{B}) : |\lambda - b_{ii}| \le R_i = \sum_{j=1, j\neq i}^{n} |b_{ij}|, \, i = 1, \, 2, \, \ldots, \, n \tag{9}$$

Here, R_i are the radii of the Gerschgorin circles related to matrix $\boldsymbol{B} = (b_{ij})$. b_{ii} are centers of the Gerschgorin circles. Then, n eigenvalues of matrix $\boldsymbol{B}$ will be distributed within the union sets of the n Gerschgorin circles $G_i(\boldsymbol{B})$, i.e., $\lambda(\boldsymbol{B}) \subseteq \cup_{i=1}^{n} G_i(\boldsymbol{B})$.

According to the Gerschgorin circle theorem, the distribution equations relative to the dynamics system of the 3-RPR PM represented by Equation (6) in the vicinity of the singular point are

$$\begin{cases} b_{11} = & (3.047\cos\alpha_1 + 3.367\sin\alpha_1)F_1 + (1.23\cos\alpha_2 + 33.64\sin\alpha_2)F_2 + (3.047\cos\alpha_3 - 2.691\sin\alpha_3)F_3 \\ & -1.344 \times 10^{-12} + 2.555\dot{\theta}^2 \\ R_1 = & -(1.843\cos\alpha_1 + 2.035\sin\alpha_1)F_1 - (7.86\cos\alpha_2 + 20.35\sin\alpha_2)F_2 - (1.843\cos\alpha_3 - 1.628\sin\alpha_3)F_3 \\ & -1.927 \times 10^{-12} - 1.545\dot{\theta}^2 \\ b_{22} = & -(0.0837\cos\alpha_1 + 2.2\sin\alpha_1)F_1 + (0.105\cos\alpha_2 - 1.873\sin\alpha_2)F_2 - (0.084\cos\alpha_3 - 1.547\sin\alpha_3)F_3 \\ & +15.509\dot{\theta}^2 - 809.99 \\ R_2 = & (0.125\cos\alpha_1 + 3.274\sin\alpha_1)F_1 - (0.156\cos\alpha_2 - 2.788\sin\alpha_2)F_2 + (0.125\cos\alpha_3 + 2.302\sin\alpha_3)F_3 \\ & -23.085\dot{\theta}^2 + 1.205 \times 10^3 \\ b_{33} = & (0.845\cos\alpha_1 + 3.657\sin\alpha_1)F_1 - (1.056\cos\alpha_2 - 0.366\sin\alpha_2)F_2 + (0.845\cos\alpha_3 - 2.93\sin\alpha_3)F_3 \\ & -\dot{\theta}^2 + 5.017 \times 10^{-12} \\ R_3 = & (0.791\cos\alpha_1 + 3.426\sin\alpha_1)F_1 - (0.989\cos\alpha_2 - 3.426\sin\alpha_2)F_2 + (0.791\cos\alpha_3 - 2.74\sin\alpha_3)F_3 \\ & +4.45 \times 10^{-12}\dot{\theta} - 2.736 \times 10^{-12}\dot{\theta}^2 + 10^{-15}(6.711\dot{x}_c + 5.903\dot{y}_c)\dot{\theta} \end{cases} \tag{10}$$

In the expressions above, the velocity of the movable platform's mass center, $(\dot{x}_c, \dot{y}_c)$, minimally impacts the PM's motion stability at the singular configuration. For this reason, in the subsequent study, the velocity of the mass center is disregarded.

According to the Lyapunov criterion, if each eigenvalue of the linear approximation for the PM dynamic system has a negative real part at a singular configuration, then the motion of the dynamic system at a singular configuration is stable. Therefore, for the PM to exhibit stable motion at singular configurations, it must satisfy the following conditions:

$$b_{ii} < 0, -b_{ii} > R_i, i = 1, 2, 3 \tag{11}$$

The corresponding inequations are

$$\begin{cases} G_1 = \dot{\theta}_c^{\,2} \ge 40.24 \\ G_2 = F_2\cos(0.334 + \alpha_2) < 86F_3\cos(1.290 + \alpha_3) \\ G_3 = F_2\cos(0.334 + \alpha_2) < -3.75F_1\cos(1.344 - \alpha_1) \\ G_4 = F_1\cos(1.533 - \alpha_1) + 0.296F_2\cos(1.515 + \alpha_2) + 0.896F_3\cos(1.517 - \alpha_3) < 0.563\dot{\theta}_c^{\,2} \end{cases} \tag{12}$$

Equation (12) unequivocally confirms that the motion stability of the 3-RPR PM at singular configurations is entirely independent of the velocity of the mass center of the movable platform, or any minimal relationship. Therefore, in the follow-up study, the velocity of the mass center is disregarded. Nonetheless, the revealed inequality, $\dot{\theta}_c^{\,2} \ge 40.24$, holds great significance in guiding the trajectory design of the PM. It hints that only when the angular speed of the movable platform is more significant than a specific value can the

dynamics system of the 3-RPR PM obtain stable motion at singular configurations. The higher the angular speed is, the better its motion stability at singular configurations is. This result is consistent with the conclusion in [35].

3.2.3. External Loads

The external loads $\vec{F}_i$ (including amplitude F_i and direction α_i in Equation (12)) are the minimum load capacities to meet the requirements of the motion stability at singular configurations. From the fourth inequation of Equation (12), it can be observed that when the load direction is determined, without the loss of generality, for instance, $\alpha_1 = 1.5327\,(\text{rad})$, $\alpha_2 = -1.5145\,(\text{rad})$, $\alpha_3 = 1.5167\,(\text{rad})$, and the loads along the acting directions are restricted by

$$F_1 + 0.2958F_2 + 0.896F_3 < 0.5628\dot{\theta}_c{}^2 = 0.5628 \times 40.24$$

However, the load capacities along the opposite directions of the acting forces have no restriction, such as $F_i = -F_i$. In this situation, the statement [39] that PMs cannot bear the external loads along the gained DoF at singular configurations is not valid; it should be modified as PMs cannot bear the external loads along a specific direction of the gained DoF at singular configurations; however, in the opposite direction of the specific direction of the gained DoF, the load capability of the PMs cannot be affected. The new finding here that, in the opposite direction of the specific direction of the gained DoF, the load capability of PMs cannot be affected is significant for expanding applications of PMs and improving their performance in the whole workspace in which singular configurations exist. For instance, the singularity may be eliminated if the external loads act in the opposite direction of the specific direction of the gained DoF through trajectory planning in the design or practical control stage. The direction in which the degree of freedom is gained should be pre-analyzed individually for specific PMs.

Equation (12) has seven variables. Adjusting these kinematic parameters in the trajectory stage makes it easy to obtain the distributions of the movable platform's velocity and angular speed that meet the motion stability at singular configurations corresponding to the specific load capability. For instance, while $\alpha_1 = 1.533\,(\text{rad})$, $\alpha_2 = -1.515\,(\text{rad})$, and $\alpha_3 = 1.517\,(\text{rad})$, the distributions of the external loads that meet the motion stability at singular configurations are shown in Figure 3a. When external loads are positioned within the inner space surrounded by π_1, π_2, π_3, the PM can produce stable motion even at a singular configuration. Increasing the angular speed of the movable platform can expand the range of external loads that meet the motion stability at singular configurations, as shown in Figure 3b.
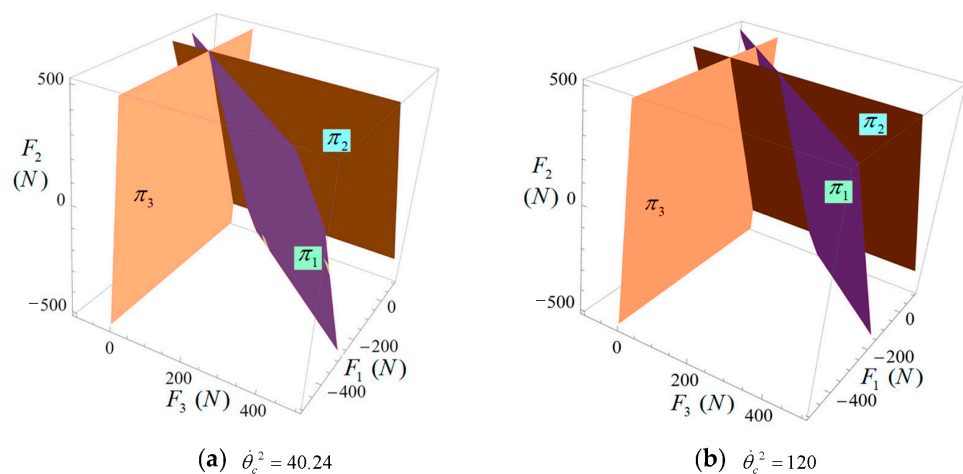

Figure 3. Distributions of the external loads meeting the motion stability at singular configurations.

3.3. Improving Motion Stability at Singular Configuration

3.3.1. Hurwitz Criterion

When all the eigenvalues obtained from Equation (12) fall within the negative real axis space, the Gerschgorin circle theorem can be utilized to reliably determine external loads that conform to the criteria for motion stability. Nonetheless, this method's stringent nature may result in the exclusion of eigenvalues with negative real parts that partially intersect with the Gerschgorin circles in the negative real part space. In contrast, the Hurwitz criterion, an exact method providing necessary and sufficient conditions for ascertaining the negativity of eigenvalues' real parts, is employed to assess the influence of the external loads, velocity, and angular speed of the movable platform on the PM's motion stability.

For the polynomial equation of the eigenvalues shown in Equation (8), the necessary and sufficient condition for each of the eigenvalues having a negative real part is $\Delta_k > 0$, $k = 1, 2, \cdots, n$. The three inequations related to $n = 3$ are

$$\Delta_1 = C_2 > 0, \ \Delta_2 = \begin{vmatrix} C_2 & C_0 \\ 1 & C_1 \end{vmatrix} > 0, \ \Delta_3 = \begin{vmatrix} C_2 & C_0 & 0 \\ 1 & C_1 & 0 \\ 0 & C_2 & C_0 \end{vmatrix} > 0 \tag{13}$$

Here, $C_2 = F_1 \cos(0.903 - \alpha_1) + 0.0.199 F_2 \cos(1.281 + \alpha_2) + 1.32 F_3 \cos(1.082 + \alpha_3) - 2.94 \dot{\theta}_c{}^2 + 131.82$.

$$\begin{aligned} C_1 &= \sum_{i=1}^{3} \tau_i F_i^2 + 0.817 \dot{\theta}_c^2 - 0.018 \dot{\theta}_c^4 + 10^{-4}(8.58 \dot{x}_c - 9.413 \ddot{y}_c) \dot{\theta}_c^3 - 10^{-2}(4.15 \dot{x}_c - 4.014 \dot{y}_c) \dot{\theta}_c \\ &+ \sum_{i=0}^{3} v_{i+3} F_i) + F_2(\varsigma_0 \dot{\theta}_c^2 + (\varsigma_1 \dot{x}_c + \varsigma_2 \dot{y}_c) \dot{\theta}_c + \sum_{i=0}^{3} \varsigma_{i+3} F_i) + F_3(\zeta_0 \dot{\theta}_c^2 + (\xi_1 \dot{x}_c + \xi_2 \dot{y}_c) \dot{\theta}_c + \sum_{i=0}^{3} \xi_{i+3} F_i) \\ &+ 27.802 + (v_1 \dot{x}_c + v_2 \dot{y}_c) \dot{\theta}_c + F_1(v_0 \dot{\theta}_c^2) \end{aligned}$$

$$C_0 = p_0 F_1 F_2 F_3 + \sum_{i=1}^{3} p_i F_i^3 + \sum_{i=1}^{3} \sum_{j=1}^{3} q_{ij} F_i^2 F_j + \dot{\theta}_c^2 \sum_{i=1}^{3} \sum_{j=1}^{3} u_{ij} F_i F_j + \dot{\theta}_c^4 \sum_{i=1}^{3} v_i F_i$$

and $p, q, \tau, v, \xi, \zeta$ are coefficients relative to the acting directions α_i of the external forces.

The inequation relative to $\Delta_1 = C_2 > 0$ is

$$F_1 \cos(0.90 - \alpha_1 + \pi) + 0.2 F_2 \cos(1.28 + \alpha_2 + \pi) + 1.32 F_3 \cos(1.08 + \alpha_3 + \pi) < 131.8 - 2.94 \dot{\theta}_c{}^2 \tag{14a}$$

Two inequations, $C_2 \cdot C_1 - C_0 > 0$ and $C_2 \cdot C_1 \cdot C_0 - C_0 \cdot C_0 > 0$, related to $\Delta_1 > 0$, $\Delta_2 > 0$ are equivalent to $C_0 > 0$ and $C_2 \cdot C_1 - C_0 > 0$. The expression of $C_0 > 0$ is

$$p_0 F_1 F_2 F_3 + \sum_{i=1}^{3} p_i F_i^3 + \sum_{i=1}^{3} \sum_{j=1}^{3} q_{ij} F_i^2 F_j + \dot{\theta}_c^2 \sum_{i=1}^{3} \sum_{j=1}^{3} u_{ij} F_i F_j + \dot{\theta}_c^4 \sum_{i=1}^{3} v_i F_i > 0 \tag{14b}$$

The expression $C_2 \cdot C_1 - C_0 > 0$ is very complicated and long-winded. Its whole expression has more than 900 terms in Mathematica®. Here, its formal representation is

$$C_2 \cdot C_1 - C_0 = f_1(F_i^3, \dot{\theta}_c^6, \dot{x}_c, \dot{y}_c, \alpha_i) > 0 \tag{14c}$$

3.3.2. Motion Stability at the Singular Configuration with a Gained Rotation-Type DoF

Equation (12) has demonstrated that the motion stability of the 3-RPR PM at singular configurations has a minimal relation to the velocity of the movable platform's mass center. For this reason, the velocity of the mass center is neglected in the follow-up study. Let $\dot{x}_c = \dot{y}_c = 0$ without a loss of generality. The inequation (14a)–(14c) still contains six variables, F_i, α_i, $i = 1, 2, 3$. Theoretically, it should be feasible to obtain external loads that meet the dynamic stability requirements from these equations concerning the angular velocity of the movable platform.

i. Static singularity ($\dot{\theta}_c = 0$)

Assuming that the directions of the external forces are given, such as $\alpha_1 = 0.902(\text{rad})$, $\alpha_2 = -1.281(\text{rad})$, and $\alpha_3 = -1.082(\text{rad})$, the detailed expression of Equations (14a)–(14c) is as follows:

$$\Delta_1 = C_2 > 0 : \Rightarrow \quad F_1 + 0.1988F_2 + 1.3204F_3 > -131.824 > 0 \tag{15a}$$

$$\begin{aligned} \Delta_2 = C_0 > 0 :\Rightarrow \quad & 0.0496\,F_1{}^3 + 0.0935F_2{}^3 - 0.2398\,F_3{}^3 + 6.685F_1F_2F_3 \\ & + F_1^2(457.37 + 5.369F_2 - 0.2072F_3) + F_2^2(-47.61 - 1.5197F_1 - 0.7947F_3) \\ & + F_3^2(-277.01 - 0.4934F_1 + 1.732F_2) + 160.05F_1F_2 + 278.27F_2F_3 + 86.1563F_1F_3 > 0 \end{aligned} \tag{15b}$$

$$\begin{aligned} \Delta_3 = C_2 \cdot C_1 - C_0 > 0 :\Rightarrow\ & 2.251 \times 10^6 - 0.08087F_1{}^3 + 0.172F_2{}^3 + 0.305F_3{}^3 - 1.324F_1F_2F_3 \\ & - F_1^2(113.98 + 1.392F_2 + 0.599F_3) + F_2^2(-175.69 + 0.589F_1 + 1.2585F_3) \\ & - F_3^2(322.57 + 0.418F_1 - 0.8264F_2) - 154.23F_1F_2 - 531.65F_2F_3 - 322.08F_1F_3 \\ & - 411.79F_1 + 37528F_2 + 6535.58F_3 > 0 \end{aligned} \tag{16}$$

Consider that the ranges of the external loads are confined within $F_i \in \{-500(N),\ 500(N)\}$. Three external load distribution surfaces, π_1, π_2, and π_3, satisfying the requirements of the dynamic stability at static singularities corresponding to Equation (15), are shown in Figure 4a. In the π_1 plane, $\Delta_1 > 0$ is distributed along the direction of the normal $\vec{n}_1$. $\Delta_2 > 0$ is distributed in the outer space of the surface based on π_2 along the direction of the surface normal $\vec{n}_2$. As Δ_2 increases, π_2 expands outward in the $\vec{n}_2$ direction. $\Delta_3 > 0$ is distributed in the inner and outer space of the surface based on π_3 along the direction of the surface normal $\vec{n}_3$. As Δ_3 increases, the complex surface of the π_3 space shrinks inward toward $\vec{n}_3$. In the eight quadrants, π_1, π_2, and π_3 intersect only in the first quadrant. Therefore, the range that can meet the dynamic stability requirements at static singular configurations is the local space enclosed by the surfaces π_2 and π_3 in the first quadrant. Obtaining this local space with stable motion by trial-and-error numerical methods is challenging. When the values of α_i, $i = 1, 2, 3$ are altered, the intersecting distribution spaces of the external loads that satisfy dynamic stability at singularities may undergo changes or even cease to exist.

When the directions of the external forces are coaxial with the driving legs, $\alpha_1 = 1.484(\text{rad})$, $\alpha_2 = 3.752(\text{rad})$, $\alpha_3 = 2.618(\text{rad})$, there is a common load distribution region that satisfies $\Delta_i > 0$, $i = 1, 2, 3$ simultaneously, as shown in Figure 4b. When the external load is perpendicular to the driving legs, that is, when the directions of the external loads are consistent with the directions of the gained DoF, no load distribution region simultaneously satisfies $\Delta_i > 0$. Because the external load distribution region determined by $\Delta_1 > 0$ does not intersect with the load distribution region determined by $\Delta_2 > 0$, the Hurwitz stability criterion is not met. Thus, the system will exhibit an unstable motion state at singularities. This analysis result aligns with those obtained using previous numerical methods. That is, when a PM with a gained rotation-type singularity is subjected to external loads in the direction of the gained DoF at the static singular configuration, the moving platform cannot withstand the external loads.

ii. Dynamic singularity ($\dot{\theta}_c \neq 0$)

Figure 4c illustrates three load distributions that result in stable motion at a singular configuration. These distributions are associated with a gained rotation-type DoF around the instantaneous rotational center of the movable platform when $\dot{\theta}_c{}^2 = 40.24$ and the external loads act from the fixed platform to the movable platform along the driving legs. The figure depicts two intersecting regions, Ω_1 and Ω_2, associated with three inequalities from Equation (14a)–(14c) and their corresponding load distribution surfaces, π_1, π_2, and π_3. The Ω_1 region gradually expands from the load center, aligning with the result obtained using the Gerschgorin circle theorem. This suggests that when the angular speed of the movable platform exceeds a specific value, the system still meets the motion stability requirements at singular configurations, even when the external loads are zero.

By increasing the angular speed of the movable platform, the PM's load capability to meet motion stability at singular configurations in the Ω_1 region is enhanced, as shown in Figure 4d.

Similar load distribution results can be observed when the external forces are perpendicular to the input leg axes. However, by adjusting the velocity of the movable platform's mass center, $(\dot{x}_c, \dot{y}_c)$, the external load distributions that meet the motion stability at singular configurations are almost maintained. For other singular configurations of the 3-RPR PM with a rotation-type DoF [38], the external load distributions ensuring motion stability at singular configurations are similar to those depicted in Figure 4. Increasing the angular speed of the movable platform is an effective method to improve the PM's motion stability at the singular configuration once the angular speed surpasses a specific threshold.
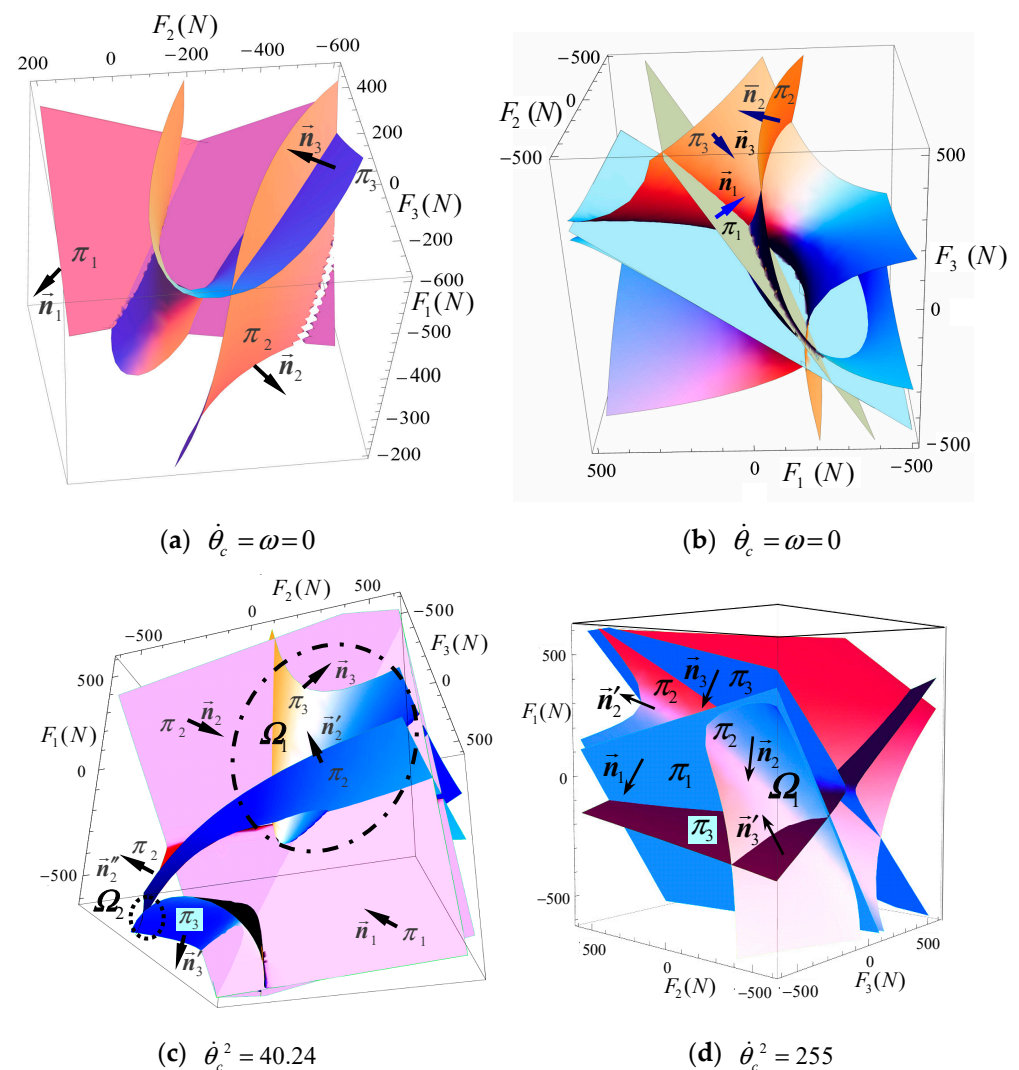

Figure 4. Distributions of external loads at the singular configurations with a gained rotation-type DoF.

3.3.3. Motion Stability at the Singular Configuration with a Gained Translation-Type DoF

For the singular configuration $(x_{c0}, y_{c0}, \theta_{c0}) = (0.3646, 0.45, 40\deg)$ [38] with a gained translation-type DoF for the 3-RPR PM, a specific external load distribution region Ω_1 satisfying $\Delta_i > 0$ simultaneously related to $\alpha_1 = 1.072\,(\text{rad})$, $\alpha_2 = 0.135\,(\text{rad})$, and $\alpha_3 = -1.076\,(\text{rad})$ is depicted in Figure 5a. As the velocity of the movable platform increases in the direction of the gained translation-type DoF, $[\dot{x}_c/\dot{y}_c = \tan(40\deg)]$, the external load distribution region Ω_1, satisfying $\Delta_i > 0$, gradually diminishes until it vanishes. A similar external load distribution feature for the region Ω_1 can be observed when increasing the

velocity of the movable platform perpendicular to the gained translation-type DoF. Increasing the angular velocity of the movable platform, the external load distribution region Ω_1 with $\Delta_i > 0$ gradually shrinks until it disappears, or a shared intersection region appears on a larger external load space.

(**a**) $\dot{\theta}_c^2 = 40.24$, $\dot{x}_c = 0$, $\dot{y}_c = 0$
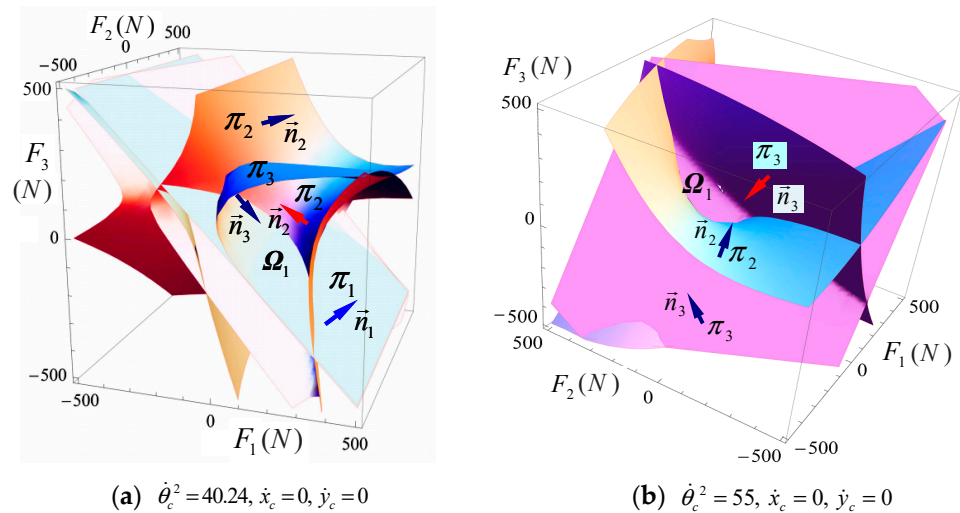(**b**) $\dot{\theta}_c^2 = 55$, $\dot{x}_c = 0$, $\dot{y}_c = 0$

Figure 5. Distributions of external loads meeting $\Delta_i > 0$, $i = 1, 2, 3$ at the singular configuration with one gained translation-type DoF..

When the external loads are perpendicular to the driving leg axes, the approximate expression for $\Delta_1 > 0$ is $\dot{\theta}_c^2 > 54.489$. Figure 5b depicts the external load distributions meeting both $\Delta_2 > 0$ and $\Delta_3 > 0$ simultaneously. In this figure, the region Ω_1 representing the external load distribution meeting $\Delta_i > 0$ is relatively larger. As a result, the 3-RPR PM can achieve a greater motion stability at the singular configuration.
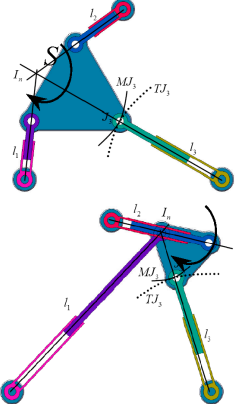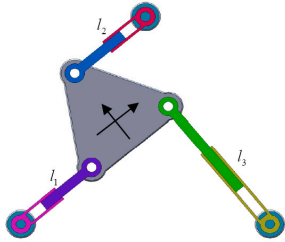
3.4. Summary of New Findings for Singularly Properties

It is essential to comprehend the dynamic characteristics and influence mechanisms of kinematic parameters and external loads on the system's stability at singularities. This understanding is necessary to address the PM's dynamic singularity-free issue by thoroughly elucidating the PM's dynamic characteristics at singularities. For a long time, scholars have primarily concentrated on examining singularity avoidance issues associated with the first type of static singularities ($\dot{l}_i = \ddot{l}_i = 0$ and $v_i = 0$) while neglecting to address other static singularities, such as the second ($\mu_i = \dot{l}_i^2 + l_i\ddot{l}_i = 0$, $\dot{l}_i \neq 0$, $\ddot{l}_i \neq 0$ and $v_i = 0$) and third types ($\mu_i = v_i$, $\mu_i \neq 0$, $v_i \neq 0$; then, $q_{bi} = m_i(\mu_i - v_i) = 0$). Consequently, there has been minimal investigation into the dynamic stability of PMs at singular points under external loads within the current body of literature. The artificial potential function in [25] and reconfigurable active masses in [23,24] have explicitly and implicitly considered the effect of kinematic parameters on PMs' motion stability to modify PMs' dynamic behaviors at singular configurations. However, the mechanism to improve PMs' dynamic behaviors, including motion stability at singular configurations, has yet to be studied in the existing literature.

In order to address the research gap in this area, which is currently lacking any literature that takes into account the dynamic characteristics of the system when developing singularity-free methods and exploring PMs' motion stability at singularities, this paper conducts a theoretical analysis of the spatial distribution surfaces where PMs meet the dynamic stability criteria at singularities related to kinematic parameters and external loads. From the perspective of dynamic stability, the theoretical analysis achieved in this paper, based on the Gerschgorin perturbation approach and the Hurwitz exact approach, has

led to many discoveries beyond previous numerical methods. The information in Table 1 provides a summary of some noteworthy new discoveries.

Table 1. Summary of new findings for singularity properties related to kinematic parameters and external forces.

Type of the Gained DoF	Static Singularity	Dynamic Singularity
Rotation-type	$\dot{l}_i = \ddot{l}_i = 0$ and $v_i = 0$. $v_i = 0$ and $\mu_i = \dot{l}_i{}^2 + l_i\ddot{l}_i = 0; \dot{l}_i \neq 0; \ddot{l}_i \neq 0$ $\mu_i = v_i, \mu_i \neq 0, v_i \neq 0$. The PM cannot withstand the external loads acting toward the gained DoF at static singular points.	Let the platform's instantaneous center of absolute velocity be away from the singular point S. The higher the angular speed is, the better its motion stability at singular configurations is while $\theta_c \geq \omega_0$. The PM's load capability cannot be affected in the opposite direction of the gained DoF. Increasing the angular speed can enhance the PM's load capability and meet motion stability at singular points. The PM's motion stability at singularities is almost maintained related to changing the movable platform's velocity.
Translation-type		Increasing the movable platform's velocity along the gained DoF will reduce the PM's load capability with stable motion at the singularity. The PM's load capability with stable motion at the singularity will be enhanced if the external loads are perpendicular to the driving leg axes.

The primary objective of this study is to thoroughly comprehend the impact of each kinematic parameter on the PM's motion stability at singularities. The goal is to develop a more efficient and user-friendly method, specifically tailored for aerospace applications, that can dynamically and adaptively avoid singularities in real time based on sensing input parameters without requiring offline calculations. The stability analysis of nonlinear dynamical systems is complicated, especially for high-dimensional ones. PMs are typically part of high-dimensional nonlinear dynamic systems, making it more challenging to study their singularity dynamic bifurcation characteristics, based on which a new singularity avoidance method is constructed to realize real-time singularity avoidance control. The work presented in this paper aims to simplify subsequent research on PMs' dynamic bifurcation characteristics by identifying the critical kinematic parameters that influence the dynamic characteristics at singularity, and using them as bifurcation parameters. To the best of the author's knowledge, no existing literature has considered the system's dynamic characteristics when constructing singularity-free approaches and studying PMs' stability at singularities.

The theoretical analysis results presented in Table 1 have led to many discoveries beyond previous numerical methods, besides confirming the significant impact of kinematic parameters on the PM's motion stability at singular configurations. For instance, it has been found that changing the velocity of the mass center of the movable platform is a simple and effective method to enhance the PM's motion stability at singular configurations. Some commonly accepted statements in prior research, such as the statement that PMs cannot support external loads in the direction of the gained DoF at singular configurations [39], are only partially accurate. It has been found that PMs' load capacity is not affected when the load is applied in the opposite direction of the gained DoF. The effects of the kinematic

parameters on the PM's motion stability at singular configurations revealed in this paper will pave the way for a new singularity-free method for realizing PMs' adaptive and robust singularity-free control by detecting kinematic parameters without introducing redundancy or active mass.

4. Discussion

In aerospace engineering, it is essential to enhance PMs' accuracy in practical operations and improve their dexterity and adaptability in planning and tracking workspace trajectories. This investigation aims to comprehensively elucidate the influence of kinematic parameters on a PM's motion stability at singularities, aiming at developing a more agile and adaptive singularity-free approach tailored for aerospace applications without requiring offline calculations. Thus, the PM's singularities can be swiftly eliminated based on sensing input parameters.

Studying the dynamic behaviors of PMs is challenging due to the complex issue of Jacobian matrix rank reduction near singularities. Consequently, there is a scarcity of literature on the investigation of PMs' dynamic behaviors near singularities and the influence of kinematic parameters on the motion stability of PMs. The present paper utilizes Lyapunov's dynamic stability theory to explore a PM's dynamic stability at singularities and how kinematic parameters influence it. With the linear approximation of the PM dynamic system near the singular point and the perturbation analysis method, this pioneering study addresses a research gap by providing insight into the limited research and understanding of PM's dynamic behaviors at singularities and their relation to kinematic parameters in the academic community. The proposed theoretical analysis has led to many discoveries beyond previous numerical methods. Two new types of static singularities have been discovered for the first time, and some important dynamic characteristics and influence mechanisms of kinematic parameters and external loads on the PM's dynamic stability at singularities have been revealed.

In aerospace applications, addressing the real-time, robust, and reliable singularity avoidance of PMs is of the utmost importance. The authors have been dedicated to developing a new method to solve this issue over an extended period. The artificial potential function in [25] and reconfigurable active masses in [23,24] have explicitly and implicitly considered the effect of kinematic parameters on PMs' motion stability to modify their dynamic behaviors at singular configurations. However, the mechanism to improve PMs' dynamic behaviors, including motion stability at singular configurations, has yet to be studied in the existing literature. Francisco et al. [3] developed an approach that allows the PM to follow the trajectory and avoid singular configurations while keeping the actuator forces to a minimum by reconfiguring the mobile and fixed platforms via changing the anchoring points' locations on both platforms. A prototype was created to quickly test the reconfiguration strategy, where anchoring points are moved to holes drilled in the fixed and mobile platforms to enable reconfiguration by adjusting their position. Baron et al. [4] developed a robust geometric method to prevent singularities in a redundant planar PM by utilizing the properties of the instantaneous centers of rotation (ICRs). This approach offers the advantage of being able to quantify a PM's proximity to a singularity using a physical distance, and it enables the PM to move away from a singular configuration by minimizing the radius through sub-mechanism reconfiguration in terms of a redundant variable. Refs [3,4] enhance singular avoidance robustness but may require sacrifices, such as redundant DoFs or components, resulting in control bias near the singular configuration. Moreover, optimization is essential for implementing singularity-free control processes, so these methods still need improvement to achieve real-time control. Specifically, recalculating singularity and its spatial distribution is essential when pose parameters are changed because the identified singularity is closely related to the pose parameters of the moving platform. Therefore, the singularity avoidance method's adaptivity should be enhanced.

The stability analysis of nonlinear dynamical systems is complicated, especially for high-dimensional ones. PMs are typically part of high-dimensional nonlinear dynamic systems, making it more challenging to study their singularity dynamic bifurcation characteristics, based on which a new singularity avoidance method is constructed to realize real-time singularity avoidance control. The work proposed in this paper aims to simplify subsequent research on PMs' dynamic bifurcation characteristics by identifying the critical kinematic parameters that influence the dynamic characteristics at singularity, and using them as bifurcation parameters. To the best of the author's knowledge, no existing literature has considered the system's dynamic characteristics when constructing singularity-free approaches and studying a PM's stability at singularities.

The research method proposed in this paper is universal since any PM can be discretized into a particle system, and the consistency of the kinematic parameters influences dynamic motion stability at singular configurations. Some of the new findings listed in Table 1 may also be applicable to other PMs. However, due to the significant differences in PMs' dynamic characteristics, individual research is necessary to obtain the primary kinematic parameters affecting PMs' dynamic stability and construct the corresponding singularity-free algorithm.

In our future work, we plan to use a holistic design methodology to develop a new approach for achieving real-time singularity-free control, considering the system's dynamic characteristics and sensor-based real-time control while comprehensively considering the effects of the kinematic parameters on motion stability. By inspecting the system's kinematic parameters, the approach can guide a PM to pass by singular configurations with robustly stable motion in the real-time control model without introducing redundancy or active mass. This approach benefits PMs in aerospace engineering, ensuring the safety of aerospace devices equipped with PMs by avoiding redundancy or active mass.

5. Conclusions

The analytical approach, based on the Gerschgorin circle theorem approximate approach and the exact Hurwitz criterion approach, is applied to reveal the effect mechanisms of kinematic parameters on the motion stability of the planar 3-RPR PMs at singular configurations. The proposed theoretical analysis method has resulted in numerous discoveries beyond previous numerical methods, and primary kinematic parameters affecting the PM's motion stability at singular configurations are determined. Moreover, two other static singularities overlooked by scholars have been revealed. The research gap in the limited literature and the understanding of PMs' dynamic behaviors at singularities and their relation to kinematic parameters in the academic community due to the complex issue of Jacobian matrix rank reduction near singularities has been filled. The findings in this paper about how the kinematic parameters impact PMs' motion stability at singular configurations will pave the way for developing a new method to realize PMs' adaptive and robust singularity-free control by detecting kinematic parameters without introducing redundancy or active mass.

Author Contributions: Methodology and software, Y.-T.L.; conceptualization and writing, review and editing, Y.-X.W. All authors have read and agreed to the published version of the manuscript.

Data Availability Statement: The data used in this study comes from internal modeling software that cannot be publicly accessed. Unfortunately, we cannot publicly share the data generated by this software.

Conflicts of Interest: The authors declare no conflicts of interest. The funders had no role in the design of the study; in the collection, analyses, or interpretation of the data; in the writing of the manuscript; or in the decision to publish the results.

Nomenclature

P	Prismatic pair in mechanism. 2-RPR PM is a PM with two branches consisting of RPR joints.
S	Spherical pair in mechanism. RPR is a branch with two R pairs at ends and a P pair in middle.
R	Revolute pair in mechanism. 3-RPR PM is a PM with three branches consisting of RPR joints.
A_i	Three revolute joints $(i = 1, 2, 3)$ on the base.
B_i	Three revolute joints $(i = 1, 2, 3)$ on the movable platform.
m_i	Discrete concentrated masses located at B_i, $(i = 1, 2, 3)$.
a	The length from A_1 to A_3.
a_0, b_0	The horizontal and vertical coordinates of A_2.
b_i	Distance between two neighboring revolute joints on the movable platform.
m_4, m_7	Two concentrated masses of two components of the prismatic pair P_1 related to the input parameter l_1.
l_i	Input parameters, or lengths of legs l_i, $(i = 1, 2, 3)$.
c_1	The distance from $m_1(C_1)$ to $m_4(B_1)$.
d_1	The distance from $m_7(D_1)$ to A_1.
x_c, y_c	The mess center coordinates of the movable platform.
x_{c0}, y_{c0}	Singularity coordinates of 3-RPR PM.
x_0, y_0	Instantaneous velocity center of the movable platform.
$\vec{F}_i$	External forces act on the movable platform through joints B_i.
α_i	Acting angles of $\vec{F}_i$ related to the horizontal axis x.
$\zeta = [\zeta_i]_{i=1,\dots,12}^{12}$	Lagrange multiplier.
$\dot{l}_i, \ddot{l}_i$	The velocities and accelerations of the input kinematic parameters.
μ_i	Input kinematic parameters, $\mu_i = \dot{l}_i{}^2 + l_i \ddot{l}_i$, $(i = 1, 2, 3)$.
v_i	Kinematic parameters related to joint velocities, $v_i = \dot{x}_i{}^2 + \dot{y}_i{}^2$.
A	The eigenvalue matrix of the first-order nonlinear differential dynamics system of the planar 3-RPR PM.
λ	Eigenvalue determined by matrix A.

Appendix A

$$[A_{rs}] = \begin{bmatrix} A_{1,1} & \cdots & A_{1,18} \\ \vdots & \ddots & \vdots \\ A_{12,1} & \cdots & A_{12,18} \end{bmatrix} = \begin{bmatrix} \frac{\partial f_1}{\partial x_1} & \frac{\partial f_1}{\partial y_1} & \frac{\partial f_1}{\partial x_2} & \frac{\partial f_1}{\partial y_2} & \cdots & \frac{\partial f_1}{\partial y_8} & \frac{\partial f_1}{\partial x_9} & \frac{\partial f_1}{\partial y_9} \\ \frac{\partial f_2}{\partial x_1} & \frac{\partial f_2}{\partial y_1} & \frac{\partial f_2}{\partial x_2} & \frac{\partial f_2}{\partial y_2} & \cdots & \frac{\partial f_2}{\partial y_8} & \frac{\partial f_2}{\partial x_9} & \frac{\partial f_2}{\partial y_9} \\ \cdots & \cdots & & & & \cdots & & \cdots \\ \frac{\partial f_{12}}{\partial x_1} & \frac{\partial f_{12}}{\partial y_1} & \frac{\partial f_{12}}{\partial x_2} & \frac{\partial f_{12}}{\partial y_2} & \cdots & \frac{\partial f_{12}}{\partial y_8} & \frac{\partial f_{12}}{\partial x_9} & \frac{\partial f_{12}}{\partial y_9} \end{bmatrix}$$

References

1. Pulloquinga, J.L.; Escarabajal, R.J.; Valera, Á.; Vallés, M.; Mata, V. A Type II singularity avoidance algorithm for parallel manipulators using output twist screws. *Mech. Mach. Theory* **2023**, *183*, 105282. [CrossRef]
2. Li, C.Y.; Angeles, J.; Guo, H.W.; Yan, H.Y.; Tang, D.; Liu, R.Q.; Deng, Z.Q. Mobility and singularity analyses of asymmetric multi-loop mechanism for space applications. *Proc. Inst. Mech. Eng. Part. C J. Mech. Eng. Sci.* **2021**, *235*, 6205–6218. [CrossRef]
3. Francisco, V.; Miguel, D.R.; Marina, V.; Antonio, B.; Enrique, B.; Ánge, V. Reconfiguration of a parallel kinematic manipulator with 2T2R motions for avoiding singularities through minimizing actuator forces. *Mechatronics* **2020**, *69*, 102382.
4. Baron, N.; Philippides, A.; Rojas, N. A robust geometric method of singularity avoidance for kinematically redundant planar parallel robot manipulators. *Mech. Mach. Theory* **2020**, *151*, 103863. [CrossRef]
5. Ghaedrahmati, R.; Gosselin, C. Kinematic analysis of a new 2-DOF parallel wrist with a large singularity-free rotational workspace. *Mech. Mach. Theory* **2022**, *175*, 104942. [CrossRef]
6. Liu, Y.Z.; Wu, J.; Wang, L.P.; Wang, J.S. Determination of the maximal singularity-free zone of 4-RRR redundant parallel manipulators and its application on investigating length ratios of links. *Robotica* **2016**, *34*, 2039–2055. [CrossRef]
7. Kaloorazi, M.F.; Masouleh, M.T.; Caro, S. Determination of the maximal singularity-free workspace of 3-DOF parallel mechanisms with a constructive geometric approach. *Mech. Mach. Theory* **2015**, *84*, 25–36. [CrossRef]
8. Zhang, W.; Zhang, W.X.; Shi, D.; Ding, X.L. Design of hip joint assistant asymmetric parallel mechanism and optimization of singularity-free workspace. *Mech. Mach. Theory* **2018**, *122*, 389–403. [CrossRef]
9. Nag, A.; Bandyopadhyay, S. Singularity-free spheres in the position and orientation work spaces of Stewart platform manipulators. *Mech. Mach. Theory* **2021**, *155*, 104041. [CrossRef]

10. Abbasnejad, G.; Daniali, H.M.; Kazemi, S.M. A new approach to determine the maximal singularity-free zone of 3-RPR planar parallel manipulator. *Robotica* **2012**, *30*, 1005–1012. [CrossRef]

11. Gola, P.; Shende, A.D.; Patra, B.; Bandyopadhyay, S. *A Comprehensive Analytical Study of the Singularity-Free Regions inside the Workspace of the 3-RPS Spatial Parallel Manipulator*; Elsevier: Amsterdam, The Netherlands, 2023.

12. Sirichotiyakul, W.; Patoglu, V.; Satici, A.C. Efficient singularity-free workspace approximations using sum-of-squares programming. *J. Mech. Robot.* **2020**, *12*, 061004. [CrossRef]

13. Bandyopadhyay, S.; Ghosal, A. Geometric characterization and parametric representation of the singularity manifold of a 6-6 Stewart platform manipulator. *Mech. Mach. Theory* **2006**, *41*, 1377–1400. [CrossRef]

14. Dash, A.K.; Chen, I.M.; Yeo, S.H.; Yang, G.L. Workspace generation and planning singularity-free path for parallel manipulators. *Mech. Mach. Theory* **2005**, *40*, 776–805. [CrossRef]

15. Liu, S.; Qiu, Z.C.; Zhang, X.M. Singularity and path-planning with the working mode conversion of a 3-DOF 3-RRR planar parallel manipulator. *Mech. Mach. Theory* **2017**, *107*, 166–182. [CrossRef]

16. Li, S.Q.; Chen, D.; Wang, J.F. An optimal singularity-free motion planning method for a 6-DOF parallel manipulator. *Ind. Robot.* **2020**, *48*, 290–299. [CrossRef]

17. Sakurai, S.; Katsura, S. Singularity-free 3-leg 6-DOF spatial parallel robot with actuation redundancy. *IEEJ J. Ind. Appl.* **2024**, *13*, 127–134. [CrossRef]

18. Liang, D.; Song, Y.M.; Sun, T.; Dong, G. Optimum design of a novel redundantly actuated parallel manipulator with multiple actuation modes for high kinematic and dynamic performance. *Nonlinear Dyn.* **2016**, *83*, 631–658. [CrossRef]

19. Corinaldi, D.; Callegari, M.; Angeles, J. Singularity-free path-planning of dexterous pointing tasks for a class of spherical parallel mechanisms. *Proc. Inst. Mech. Eng. Part. C J. Mech. Eng. Sci.* **2021**, *128*, 47–57. [CrossRef]

20. Qu, H.B.; Hu, L.Q.; Guo, S. Singularity analysis and avoidance of a planar parallel mechanism with kinematic redundancy under a fixed orientation. *Proc. Inst. Mech. Eng. Part. C J. Mech. Eng. Sci.* **2021**, *235*, 3534–3553. [CrossRef]

21. Karimi, A.; Masouleh, M.T.; Cardou, P. Avoiding the singularities of 3-RPR parallel mechanisms via dimensional synthesis and self-reconfigurability. *Mech. Mach. Theory* **2016**, *99*, 189–206. [CrossRef]

22. Gosselin, C.; Lecours, A.; Laliberte, T.; Fortin, M. Design and experimental validation of planar programmable inertia generators. *Int. J. Robot. Res.* **2014**, *33*, 489–506. [CrossRef]

23. Parsa, S.S.; Carretero, J.A.; Boudreau, R. Internal redundancy: An approach to improve the dynamic parameters around sharp corners. *Mech. Sci.* **2013**, *4*, 233–242. [CrossRef]

24. Parsa, S.S.; Boudreau, R.; Carretero, J.A. Reconfigurable mass parameters to cross direct kinematic singularities in parallel manipulators. *Mech. Mach. Theory* **2015**, *85*, 53–63. [CrossRef]

25. Agarwal, A.; Nasa, C.; Bandyopadhyay, S. Dynamic singularity avoidance for parallel manipulators using a task-priority based control scheme. *Mech. Mach. Theory* **2016**, *96*, 107–126. [CrossRef]

26. Hubert, J.; Merlet, J.P. Static of parallel manipulators and closeness to singularity. *J. Mech. Rob.* **2009**, *1*, 1–6. [CrossRef]

27. Huang, T.; Wang, M.; Yang, S.; Sun, T.; Chetwynd, D.G.; Xie, F. Force/motion transmissibility analysis of six degree of freedom parallel mechanisms. *ASME J. Mech. Robot.* **2014**, *6*, 52–68. [CrossRef]

28. Saafi, H.; Laribi, M.A.; Zeghloul, S. Forward kinematic model improveme nt of a spherical parallel manipulator using an extra sensor. *Mech. Mach. Theory* **2015**, *91*, 102–119. [CrossRef]

29. Baron, N.; Philippides, A.; Rojas, N. On the false positives and false negatives of the jacobian matrix in kinematically redundant parallel mechanisms. *IEEE Trans. Robot.* **2020**, *36*, 951–958. [CrossRef]

30. Hu, L.Q.; Gao, H.B.; Qu, H.B.; Liu, Z. Closeness to singularity based on kinematics and dynamics and singularity avoidance of a planar parallel robot with kinematic redundancy. *Proc. Inst. Mech. Eng. Part C J. Mech. Eng. Sci.* **2022**, *236*, 3717–3730. [CrossRef]

31. Yao, H.J.; Li, Q.C.; Chen, Q.H.; Chai, X.X. Measuring the closeness to singularities of a planar parallel manipulator using geometric algebra. *Appl. Math. Model.* **2018**, *57*, 192–205. [CrossRef]

32. Kapilavai, A.; Nawratil, G. Singularity distance computations for 3-RPR manipulators using extrinsic metrics. *Mech. Mach. Theory* **2024**, *195*, 105595. [CrossRef]

33. Bates, D.J.; Hauenstein, J.D.; Sommese, A.J.; Wampler, C.W. Bertini: Software for Numerical Algebraic Geometry. 2013. Available online: https://bertini.nd.edu/ (accessed on 10 May 2024).

34. Li, Y.T.; Wang, Y.X. Singularities in axisymmetric vectoring exhaust nozzle and a feasible singularity-free approach. In Proceedings of the ASME 2019 International Design Engineering Technical Conferences and Computers and Information in Engineering Conference, Anaheim, CA, USA, 18–21 August 2019. DETC2019-9812.

35. Li, Y.T.; Wang, Y.X. Effects of kinematic parameters on planar 3-RPR PM's motion stability at singular configurations. *Mech. Mach. Sci.* **2024**, *149*, 541–551.

36. Rüdiger, S. *Practical Bifurcation and Stability Analysis*; Springer: New York, NY, USA, 1994.

37. Zhang, Q.C. *Bifurcation and Chaos Theory and Its Application*; Tianjin University Press: Tianjin, China, 2005.

38. Li, Y.T.; Hong, Y.; Wang, Y.X.; Li, T.Y.; Wang, G.D. Maximal singularity-free distribution of input parameters in a parallel manipulator considering load deformations and clearances. *Proc. Inst. Mech. Eng. Part C J. Mech. Eng. Sci.* **2011**, *225*, 204–215. [CrossRef]

39. Gosselin, C.; Angeles, J. Singularity analysis of closed-loop kinematic chains. *IEEE Trans. Robot. Autom.* **1990**, *6*, 281–290. [CrossRef]